Loss of FCHSD1 leads to amelioration of chronic obstructive pulmonary disease

Takahiro Kawasaki[a,b,c,d], Fuminori Sugihara[e], Kiyoharu Fukushima[a,b,c], Takanori Matsuki[a,b,c], Hiroshi Nabeshima[a,b], Tomohisa Machida[a,b], Yuichi Mitsui[a,b,c], Saki Fujimura[d], Rio Sagawa[d], Lee Gaheun[d], Kanako Kuniyoshi[a,b], Hiroki Tanaka[a,b], Masashi Narazaki[c,f], Atsushi Kumanogoh[c,g,h], Shizuo Akira[a,b,i,1], and Takashi Satoh[a,b,d,i,1]

[a]Department of Host Defense, Research Institute for Microbial Diseases, Osaka University, 565-0871 Osaka, Japan; [b]Laboratory of Host Defense, World Premier Institute Immunology Frontier Research Center, Osaka University, 565-0871 Osaka, Japan; [c]Department of Respiratory Medicine and Clinical Immunology, Graduate School of Medicine, Osaka University, 565-0871 Osaka, Japan; [d]Department of Immune Regulation, Graduate School of Medical and Dental Sciences, Tokyo Medical and Dental University, 113-8510 Tokyo, Japan; [e]Laboratory of Biofunctional Imaging, World Premier Institute Immunology Frontier Research Center, Osaka University, 565-0871 Osaka, Japan; [f]Department of Advanced Clinical and Translational Immunology, Graduate, School of Medicine, Osaka University, 565-0871 Osaka, Japan; [g]Laboratory of Immunopathology, World Premier International Immunology Frontier Research Center, Osaka University, 565-0871 Osaka, Japan; [h]Institute for Open and Transdisciplinary Research Initiatives, Osaka University, 565-0871 Osaka, Japan; and [i]Innate Cell Therapy Inc., 530-0017 Osaka, Japan

Contributed by Shizuo Akira, April 12, 2021 (sent for review September 11, 2020; reviewed by Yasuhiko Nishioka and Masayuki Yamamoto)

Chronic obstructive pulmonary disease (COPD/emphysema) is a life-threatening disorder and there are few effective therapies. Cigarette smoke-induced oxidative stress, airway inflammation, and apoptosis of lung cells have been reported to be involved in the pathogenesis of COPD/emphysema and lead to alveolar septal destruction. Here we show that the expression level of FCH and double SH3 domains 1 (FCHSD1) was drastically increased in mice in response to elastase instillation, an experimental model of COPD. FCHSD1 is a member of the F-BAR family with two SH3 domains. We found that *Fchsd1* knockout (*Fchsd1*$^{-/-}$) mice were protected against airspace enlargement induced by elastase. Elastase-instilled lungs of *Fchsd1*$^{-/-}$ mice showed reduced inflammation and apoptosis compared with WT mice. We also found that elastase-induced reduction of Sirtuin 1 (SIRT1) levels, a histone deacetylase reported to protect against emphysema, was attenuated in the lungs of *Fchsd1*$^{-/-}$ mice. Furthermore, FCHSD1 deficiency enhanced nuclear translocation of nuclear factor-like 2 (NRF2), *a* redox-sensitive transcription factor, following H_2O_2 stimulation. Conversely, *Fchsd1* overexpression inhibited *NRF2* nuclear translocation and increased the reduction of SIRT1 levels. Notably, FCHSD1 interacted with NRF2 and SNX9. Our results show that FCHSD1 forms a multicomplex with NRF2 and SNX9 in the cytosol that prevents NRF2 from translocating to the nucleus. We propose that FCHSD1 promotes initiation of emphysema development by inhibiting nuclear translocation of NRF2, which leads to down-regulation of SIRT1.

COPD | antioxidative response | inflammation | innate immunity | FCHSD1

Chronic obstructive pulmonary disease (COPD) is a common disease worldwide with high morbidity and mortality. It is characterized by destruction of the alveolar wall and a decline in lung function (1). Pulmonary emphysema, a major component of COPD, is caused by cigarette smoking and other environmental risk factors. Emerging evidence suggests that cigarette smoke-induced oxidative stress has a critical role in the initiation phase of emphysema development. It enhances inflammation and extracellular matrix proteolysis and then enhances apoptosis of alveolar cells and septal destruction (2, 3). Oxidative stress is also involved in the development of elastase-induced emphysema (4, 5). In the progression phase, disrupted alveolar maintenance triggers apoptosis and autophagy. Disordered autophagy increases cellular stress, such as endoplasmic reticulum stress, which leads to apoptosis (6, 7). Self-amplifying injury loops involving apoptosis, oxidative stress, and inflammation further enhance disease progression (8). In addition, accelerated cell senescence in the COPD lung leads to decreased cell proliferation, which increases inflammation and reduces cell regeneration (9). However, current therapies for COPD are palliative and do not affect pulmonary cellular maintenance (10).

The acute inflammatory response of lung cells—such as epithelial cells, endothelial cells, fibroblasts, and alveolar macrophages—in COPD pathogenesis involves many intracellular signaling pathways (8). In these pathways, the activation of signaling proteins is regulated by a variety of intracellular trafficking activities and involves interactions with adaptor complexes. Molecular translocation events are thought to be driven by the generation of new protein–protein binding interactions or by second messenger-mediated binding interactions between signaling proteins and subcellular structures, while the manner by which each protein translocates from one site to another is not fully resolved (11).

Among the molecules involved in intracellular trafficking, FCH and Bin-Amphiphysin-Rvs (F-BAR) proteins belong to a class of cytosolic proteins that is primarily associated with endocytosis and vesicle trafficking (12). F-BAR proteins often contain SH3 domains, which mediate multiple interactions with endocytic, cytoskeletal, and signaling proteins (13, 14); therefore, it seems reasonable that F-BAR/SH3–containing proteins might be associated with certain diseases by modulating molecular trafficking. In fact, although the mechanisms remain unclear, emerging evidence indicates

Significance

Chronic obstructive pulmonary disease (COPD/emphysema) is a life-threatening disorder with high morbidity and mortality that is prevalent worldwide. It is characterized by destruction of the alveolar wall and a decline in lung function. However, few palliative therapies are currently available. We show that *FCH and double SH3 domains 1* (*Fchsd1*) knockout mice are protected against airspace enlargement induced by elastase. FCHSD1 deficiency enhanced nuclear translocation of *NRF2* and attenuated elastase-induced reduction in SIRT1 levels, which reduced inflammation and apoptosis of lung cells. These data indicate that FCHSD1 promotes the initiation phase of emphysema development and indicate potential therapeutic targets for COPD.

Author contributions: T.K. designed and performed the experiments; K.F., T.M., H.N., T.M., Y.M., S.F., R.S., L.G., K.K., H.T., M.N., and A.K. assisted with the experiments; F.S. performed the MRI analysis; T.S. conceptualized the project; T.K. and T.S. wrote the manuscript; and S.A. and T.S. supervised the project.

Reviewers: Y.N., Institute of Health Biosciences, University of Tokushima Graduate School; and M.Y., Tohoku University Graduate School of Medicine.

The authors declare no competing interest.

[1]To whom correspondence may be addressed. Email: sakira@biken.osaka-u.ac.jp or satoh.mbch@tmd.ac.jp.

This article contains supporting information online at https://www.pnas.org/lookup/suppl/doi:10.1073/pnas.2019167118/-/DCSupplemental.

Published June 24, 2021.

that these proteins are associated with various diseases. For example, loss of WRP is linked to impaired learning and memory in mice (15). Xiao et al. showed that FCHSD2 is a substrate for phosphorylation by ERK1/2 and regulates EGF receptor endocytic trafficking. Furthermore, the expression level of FCHSD2 is positively correlated with higher lung cancer patient survival rates (16). To investigate the molecular mechanism of COPD, we searched for COPD-related proteins, focusing on F-BAR/SH3–containing proteins. We identified the FCH domain and double SH3 domains 1 (FCHSD1). FCHSD1 is a mammalian ortholog of *Drosophila* Nervous Wreck (Nwk) and belongs to the F-BAR protein family (17). Like other F-BAR proteins, FCHSD1 is associated with certain diseases and signaling proteins (18, 19). However, to the best of our knowledge, no published study has determined the function of FCHSD1 in respiratory disease.

Here, we evaluated the role of FCHSD1 in elastase-induced emphysema and addressed whether it might regulate the initiation or progression phase of COPD and lead to lung tissue damage and emphysematous destruction.

Results

Level of FCHSD1 in the Lung Is Increased in Mice Exposed to Elastase: Generation of *Fchsd1*$^{-/-}$ Mice. To identify emphysema-related molecules, we first investigated the expression of FCH family proteins in mouse lung after elastase treatment. We found up-regulated levels of FCHSD1 in lungs in the early response stage to elastase treatment, whereas the levels of other FCH family proteins—such as CIP4, TOCA1, FER, WRP, and FCHSD2—did not change (Fig. 1*A*). We also found that FCHSD1 protein was increased in mouse type II alveolar epithelial cells (MLE-12 cells) after H_2O_2 stimulation (Fig. 1*B*). Conversely, FCHSD1 levels did not change after LPS instillation into the lungs (Fig. 1*C*). Interestingly, without stimulation, high levels of FCHSD1 were present in lungs especially in fibroblasts or epithelial cells, but not other tissues (Fig. 2 *A* and *B*). This suggested that FCHSD1 may have an important role in the lung. To determine the role of FCHSD1 in the development of pulmonary emphysema, we generated *Fchsd1* knockout (*Fchsd1*$^{-/-}$) mice, which were born at the expected Mendelian ratio (*SI Appendix*, Fig. S1 *A–C*). There was no significant difference in immune cell fraction in the spleen, bone marrow, blood, or lung (*SI Appendix*, Fig. S2), in epithelial cell or fibroblast fraction in the lung (*SI Appendix*, Fig. S2*D*), or in the gross appearance and histological morphology of these organs between *Fchsd1*$^{-/-}$ and WT mice (*SI Appendix*, Fig. S1 *D* and *E*).

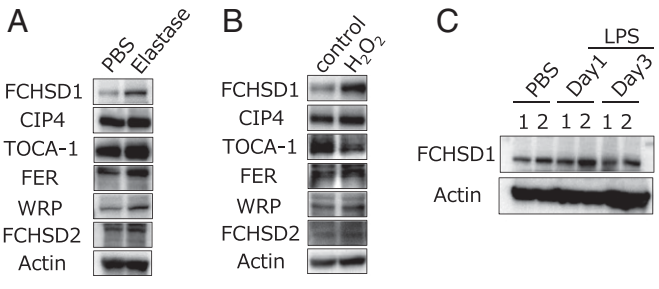

Fig. 1. Level of Fchsd1 in the lung is increased in COPD model mice. (*A*) The level of FCHSD1 and other FCH family proteins was determined by immunoblotting of mouse lung 7 d after intratracheal injection of elastase. Data are representative of at least two independent experiments. (*B*) The level of FCHSD1 and other FCH family proteins was determined by immunoblotting of MLE-12 cells exposed to 200 μM H_2O_2 for 12 h. Data are representative of at least two independent experiments. (*C*) The level of FCHSD1 in the lung was determined by immunoblotting 1 and 3 d after intratracheal injection of LPS. Data are representative of at least two independent experiments.

FCHSD1 Deficiency Protects against Pulmonary Emphysema. We exposed *Fchsd1*$^{-/-}$ and WT mice to elastase. MRI analysis revealed that *Fchsd1*$^{-/-}$ mice showed smaller areas of low opacity in the lung compared with WT mice (Fig. 2*C*). Consistent with this, histological analysis clearly indicated that *Fchsd1*$^{-/-}$ mice showed a significantly decreased mean linear intercept (MLI) and emphysematous area compared with WT mice (Fig. 2 *D–F*). However, no difference in survival or lung inflammation was observed after LPS-induced acute lung injury between *Fchsd1*$^{-/-}$ and WT mice (Fig. 2 *G–I*). These results indicate that FCHSD1 might have a crucial role in the pathogenesis of experimental elastase-induced pulmonary emphysema.

FCHSD1 Enhances Inflammation and Cell Death in Mouse Lung Exposed to Elastase. We next addressed whether the protection afforded by FCHSD1 deficiency against emphysema is associated with decreased inflammation at an early stage. *Fchsd1*$^{-/-}$ mice showed protection against acute inflammation induced by elastase, including reduced numbers of total infiltrating cells and neutrophils, and a reduced concentration of tumor necrosis factor (TNF)-α in bronchoalveolar lavage (BAL) fluid compared with similarly treated WT mice (Fig. 3 *A–C*). Consistent with this result, induction of interleukin-6 (*Il6*) and *Tnfa* mRNA was reduced in *Fchsd1*$^{-/-}$ mouse lung fibroblasts (MLFs) compared with WT MLFs in response to H_2O_2-induced oxidative stress (Fig. 3*E*). Conversely, ectopic expression of *Fchsd1* in MLE-12 cells by retroviral infection led to increased *Il6* and *Tnfa* mRNA levels following H_2O_2 stimulation compared with cells infected with empty vector (Fig. 3*H*). However, production of inflammatory cytokines, such as IL-6 and TNF-α, in response to Toll-like receptor (TLR) ligands or induction of *Il6* and *Tnfa* mRNA in response to H_2O_2 stimulation were not different between *Fchsd1*$^{-/-}$ and WT alveolar macrophages (*SI Appendix*, Fig. S3). Furthermore, TUNEL staining of the lungs after elastase treatment revealed reduced death of alveolar structural cells in *Fchsd1*$^{-/-}$ mice compared with WT mice (Fig. 3*D*). Similarly, expression of cleaved caspase 3 was reduced in *Fchsd1*$^{-/-}$ MLFs compared with WT MLFs after H_2O_2 treatment (Fig. 3*F*). In addition, acetylation of p53 at Lys382, which is a marker of apoptosis, was decreased in *Fchsd1*$^{-/-}$ MLFs compared with WT MLFs (Fig. 3*G*). Conversely, retroviral expression of *Fchsd1* in MLE-12 cells led to increased cleaved caspase 3 expression and acetylation of p53 at Lys382 in response to H_2O_2 compared with cells infected with empty vector (Fig. 3 *I* and *J*).

Collectively, these findings indicated that FCHSD1 enhances inflammation and cell death after elastase or H_2O_2 stimulation.

Loss of FCHSD1 Led to Elevation of Sirtuin 1 Levels in Lungs Exposed to Elastase and in Cells Exposed to H_2O_2. To define the function of FCHSD1 in acute lung inflammation and apoptosis, including p53 acetylation in response to elastase, we investigated the level of Sirtuin 1 (SIRT1) in lungs after elastase treatment. Consistent with previous observations (20), intratracheal injection of elastase led to a marked decrease in SIRT1 levels in the lung (Fig. 4*A*). This was attenuated in *Fchsd1*$^{-/-}$ mice compared with WT mice 24 h after intratracheal elastase treatment (Fig. 4*A*). Similarly, FOXO3a and peroxisome proliferator–activated receptor-γ (PPARγ) levels, target molecules of deacetylation by SIRT1, were higher in *Fchsd1*$^{-/-}$ mice than in WT mice exposed to elastase (Fig. 4*A*). Reduction of SIRT1 levels were attenuated in *Fchsd1*$^{-/-}$ MLFs compared with WT MLFs in response to H_2O_2 (Fig. 4*B*). Conversely, retroviral expression of *Fchsd1* in MLE-12 cells led to reduced SIRT1 levels in response to very low concentrations of H_2O_2, whereas SIRT1 levels were not reduced in response to low H_2O_2 concentrations in cells infected with empty vector (Fig. 4*C*). Together, these results confirmed a key role of FCHSD1 in the reduction of SIRT1 levels in response to oxidative stress.

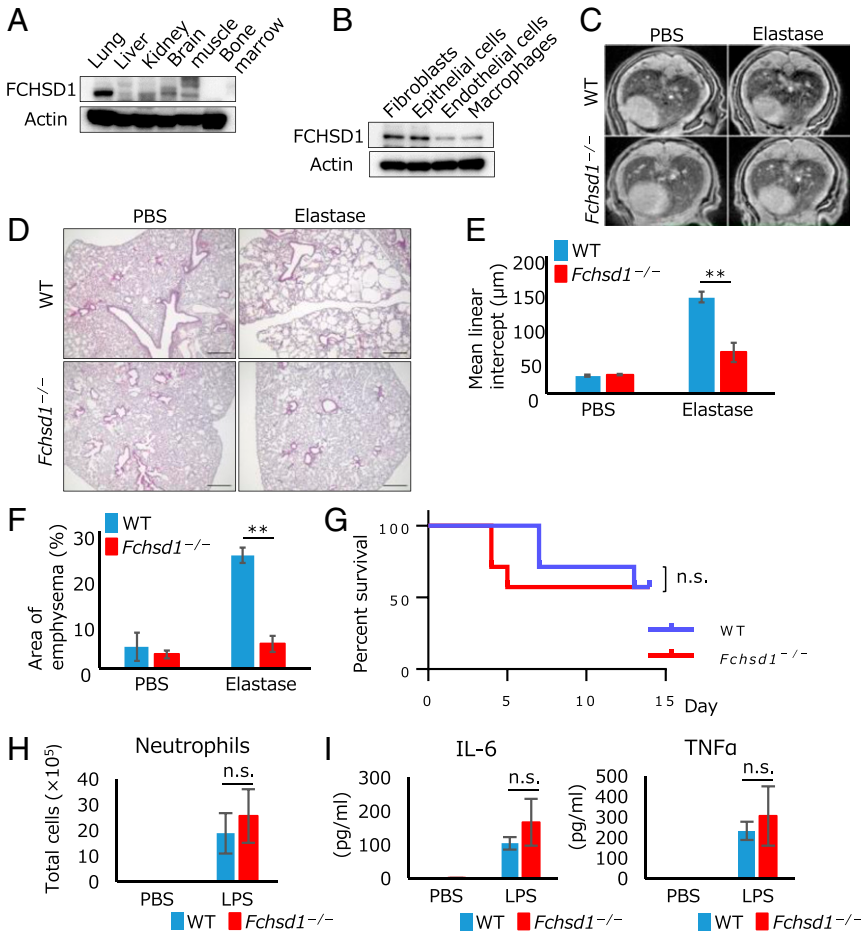

Fig. 2. FCHSD1 deficiency ameliorates elastase-induced airspace enlargement but does not alter LPS-induced inflammation and acute lung injury. (*A*) The level of FCHSD1 was determined by immunoblotting of whole-tissue homogenates from various nonstimulated mouse tissues. Data are representative of at least two independent experiments. (*B*) The level of FCHSD1 was determined by immunoblotting of primary cells sorted from nonstimulated mouse lungs. Data are representative of at least two independent experiments. (*C–F*) Morphological analysis of lungs after intratracheal injection of elastase. Lungs were collected for analysis 36 d after elastase injection. MRI images (*C*) and H&E-stained images (*D*) are representative of experiments from four separate mice. Original magnification, 4×. (Scale bars, 500 μm.) (*E*) MLI was determined by analysis using ImageJ software. (*F*) Percentage of emphysema area was determined using BZ-X Analyzer software. Both *E* and *F* were measured in H&E-stained sections of total lung. Data are expressed as the mean ± SEM. $n = 4$ per group (elastase), $n = 3$ per group (PBS). Data are representative of at least two independent experiments. (*G*) Survival of *Fchsd1*$^{-/-}$ and WT mice after intratracheal injection of LPS (10 mg/kg). $n = 7$ per group. Data are representative of at least two independent experiments. (*H* and *I*) Neutrophil number (*H*) and cytokine concentrations (*I*) in BAL fluid from *Fchsd1*$^{-/-}$ and WT mice 24 h after intratracheal treatment with LPS or PBS. $n = 4$ per group (LPS), $n = 3$ per group (PBS). Data are expressed as the mean ± SEM. Data are representative of at least two independent experiments. $^{**}P < 0.01$; n.s., not significant ($P > 0.05$).

FCHSD1 Negatively Regulates Nuclear Import of Nuclear Factor-Like 2 in Response to H_2O_2-Induced Oxidative Stress. With regard to the elastase-induced reduction of SIRT1, we next investigated the intracellular localization of nuclear factor–like 2 (NRF2), a redox-sensitive transcription factor, in response to oxidative stress. Immunoblot analysis of cytosol and nuclear fractions showed that the nuclear import of NRF2 was enhanced in *Fchsd1*$^{-/-}$ MLFs compared with WT MLFs in response to H_2O_2 treatment (Fig. 5*A*), consistent with the immunocytochemistry results (Fig. 5*C*). Conversely, retroviral expression of *Fchsd1* in MLE-12 cells led to a reduction in the nuclear import of NRF2 when similarly treated with H_2O_2 compared with cells infected with empty vector (Fig. 5 *B* and *D*). However, the mRNA level of *Nrf2* was not altered by retroviral expression of *Fchsd1* in MLE-12 cells following H_2O_2 treatment compared with cells infected with empty vector (*SI Appendix*, Fig. S4*A*). Similarly, it was also not different between *Fchsd1*$^{-/-}$ and WT MLFs in response to H_2O_2 stimulation or between lungs from *Fchsd1*$^{-/-}$ and WT mice after elastase treatment (*SI Appendix*, Fig. S4 *B* and *C*). These results indicate that FCHSD1 has a crucial role in nuclear translocation of NRF2 but does not affect the transcript level of *Nrf2*.

FCHSD1 Interacts with NRF2 and SNX9. FCHSD1 contains two SH3 domains, which mediate multiple interactions with other proteins. To further determine the function of FCHSD1 in regulating nuclear translocation of NRF2, we focused on exploring the roles of Sorting Nexin 9 (SNX9), a key interactor of FCHSD1 (21), in endocytosis and intracellular trafficking. To confirm and extend the identification of SNX9 as a FCHSD1-interacting protein, and to confirm whether FCHSD1 directly binds to NRF2, we performed coimmunoprecipitation experiments for FCHSD1, SNX9, and NRF2 in MLE-12 cells. Surprisingly, we found that FCHSD1 interacts with SNX9 and also with NRF2 (Fig. 6*A*). We next addressed whether H_2O_2 simulation alters these interactions. FCHSD1 binding to NRF2 and SNX9 was inhibited in response to H_2O_2 treatment (Fig. 6*B*). Furthermore, FCHSD1 did not associate with KEAP1 (Fig. 6*B*). In parallel, binding of SNX9 to NRF2 and Importin 8, one of the β-importins that interacts with SNX9, was promoted after H_2O_2 stimulation (Fig. 6*C*). FCHSD1 did not interact with SIRT1 or

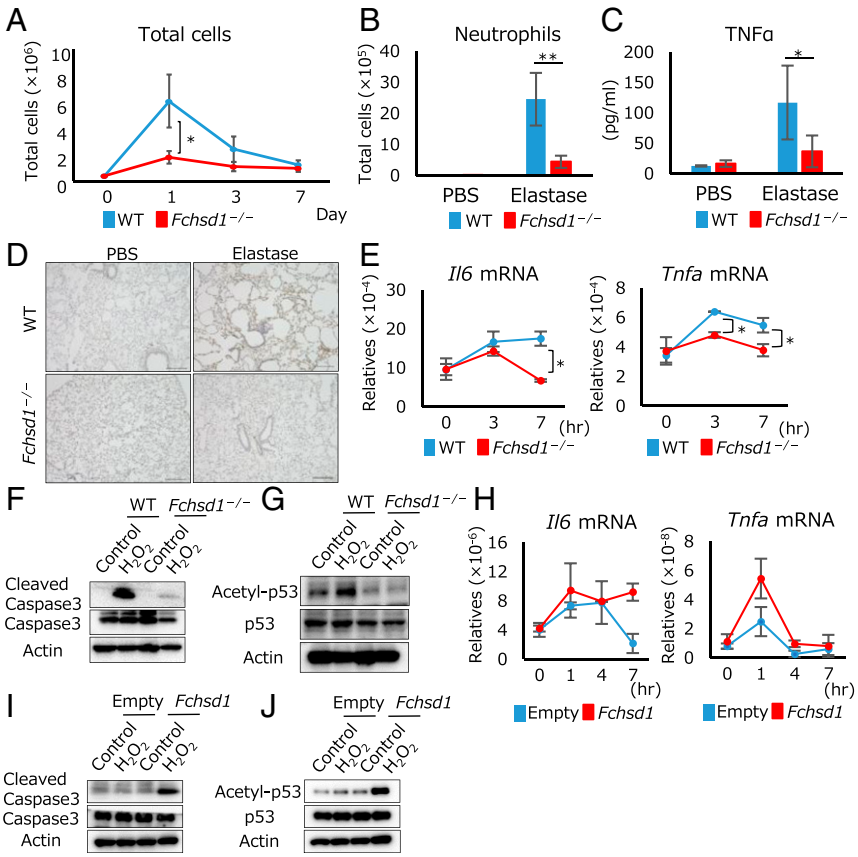

Fig. 3. FCHSD1 enhances lung inflammation and apoptosis in mice exposed to elastase. (*A*) Cell influx into BAL fluid of *Fchsd1*$^{-/-}$ and WT mice after intratracheal treatment with elastase determined by flow cytometry. $n = 4$ per group. Data are expressed as the mean ± SEM. Data are representative of at least two independent experiments. (*B*) Neutrophil number in BAL fluid of *Fchsd1*$^{-/-}$ and WT mice 24 h after intratracheal treatment with elastase determined by flow cytometry. $n = 4$ per group. Data are expressed as the mean ± SEM. Data are representative of at least two independent experiments. (*C*) TNF-α concentration in BAL fluid of *Fchsd1*$^{-/-}$ and WT mice 24 h after intratracheal treatment with elastase measured by ELISA. $n = 4$ per group. Data are expressed as the mean ± SEM. Data are representative of at least two independent experiments. (*D*) Lung sections of *Fchsd1*$^{-/-}$ and WT mice collected 24 h after elastase or PBS administration were subjected to TUNEL staining. TUNEL^{+} cells (brown) in the lung are shown. Original magnification, 10×. (Scale bars, 200 μm.) Data are representative of at least two independent experiments. (*E*) *Il6* and *Tnfa* mRNA levels in *Fchsd1*$^{-/-}$ and WT MLFs after treatment with 275 μM H_2O_2 for indicated times. Data are expressed as the mean ± SEM ($n = 3$). Data are representative of at least two independent experiments. (*F*) Immunoblot analysis of *Fchsd1*$^{-/-}$ and WT MLFs after treatment with 250 μM H_2O_2 for 12 h. Data are representative of at least two independent experiments. (*G*) Immunoblot analysis of *Fchsd1*$^{-/-}$ and WT MLFs after treatment with 50 μM H_2O_2 for 24 h. Data are representative of at least two independent experiments. (*H*) *Il6* and *Tnfa* mRNA levels in MLE-12 cells transfected with retroviral *Fchsd1* or empty control vector in response to 250 μM H_2O_2 for indicated times. Data are expressed as the mean ± SEM of duplicates ($n = 2$). Data are representative of at least two independent experiments. (*I*) Immunoblot analysis of MLE-12 cells transfected with retroviral *Fchsd1* or empty control vector after treatment with 100 μM H_2O_2 for 12 h. Data are representative of at least two independent experiments. (*J*) Immunoblot analysis of MLE-12 cells transfected with retroviral *Fchsd1* or empty control vector after treatment with 250 μM H_2O_2 for 3 h. Data are representative of at least two independent experiments. *$P < 0.05$; **$P < 0.01$; n.s., not significant ($P > 0.05$).

the indicated importins (*SI Appendix*, Fig. S5*A*). SNX9 and NRF2 did not bind to the importins (*SI Appendix*, Fig. S5 *B* and *C*). These results show that FCHSD1 interacts with NRF2 and SNX9 in the cytosol and prevents NRF2 from translocating to the nucleus. Furthermore, in response to H_2O_2 simulation, FCHSD1 dissociates from the complex and nuclear translocation of NRF2 occurs in association with increased NRF2–SNX9 and SNX9–Importin 8 interactions.

Discussion

Our findings indicate that FCHSD1 promotes the initiation phase of emphysema development by inhibiting nuclear translocation of NRF2 and then enhancing the reduction of SIRT1 levels. In a mouse model of emphysema induced by intratracheal injection of elastase, we found that deletion of *Fchsd1* protected against elastase-induced airspace enlargement, which is a characteristic feature of COPD/emphysema. Furthermore, we showed that FCHSD1 aggravated inflammation, apoptosis and down-regulation of SIRT1. With regard to the underlying mechanism, we identified protein interactions among FCHSD1, NRF2, and SNX9, and found that FCHSD1 negatively regulates nuclear translocation of NRF2 in response to oxidative stress.

Interestingly, deletion of *Fchsd1* did not protect against LPS stimulation. Consistent with this observation, FCHSD1 levels were not altered by LPS injection. This finding is in contrast to previous studies that showed protection by NRF2 and SIRT1 against LPS-induced acute lung inflammation (22–24). It is possible that the FCHSD1-SNX9-NRF2 system only has a small effect on the proinflammatory response triggered by TLR ligand stimulation in immune cells such as alveolar macrophages because the levels of the component proteins may be lower in these cells than in other cells. Further studies are needed to determine the detailed distribution of these proteins and the differentiated cell types in which the FCHSD1-SNX9-NRF2 system has a critical role in various stress responses.

NRF2 is a basic leucine zipper (bZIP) transcription factor. Following oxidative or electrophilic stress, it detaches from its cytosolic inhibitor, KEAP1, translocates to the nucleus and binds to antioxidant

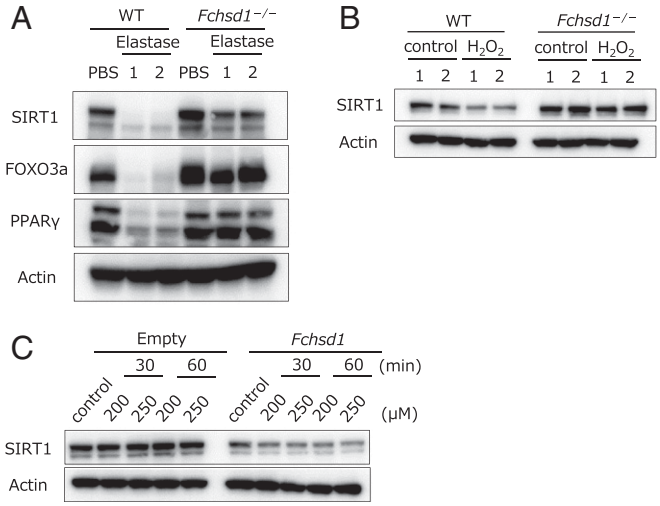

Fig. 4. Loss of FCHSD1 led to elevation of SIRT1 levels in the lung after elastase administration. The levels of indicated proteins were determined by immunoblotting of mouse lung. (*A*) Immunoblot analysis of lungs from *Fchsd1*$^{-/-}$ and WT mice 24 h after intratracheal treatment with elastase. Data are representative of at least two independent experiments. (*B*) Immunoblot analysis of *Fchsd1*$^{-/-}$ and WT MLFs after treatment with 275 μM H_2O_2 for 1 h. Data are representative of at least two independent experiments. (*C*) Immunoblot analysis of MLE-12 cells transfected with retroviral Fchsd1 or empty control vector after treatment with H_2O_2 for the indicated times. Data are representative of at least two independent experiments.

response element–containing genes (25). NRF2 is critical in determining susceptibility to lung inflammation, oxidative stress, and alveolar cell apoptosis, and disruption of the *Nrf2* gene in mice aggravates emphysema (25–27). Although the mechanism of its translocation into the nucleus is not entirely elucidated, it has been shown that NRF2 has nuclear localization signal motifs and that some importins associate with it (28). Our findings revealed that SNX9 binds to NRF2 and Importin 8 in response to oxidative stress, while FCHSD1 binds to SNX9 and NRF2. This observation indicates that FCHSD1 negatively regulates NRF2 nuclear translocation via complex formation with SNX9 and NRF2. This role of FCHSD1 may be independent of KEAP1 because we did not find direct interaction between FCHSD1 and KEAP1 during H_2O_2 stimulation. We also showed that FCHSD1 expression was increased in response to oxidative stress, which is expected to act as a brake to stop the excessive oxidative stress response. Such regulation may contribute to maintaining redox homeostasis because excessive activation of NRF2 causes reductive stress and leads to disorders such as cardiomyopathy and liver injury (29, 30).

We found that administration of elastase in vivo and H_2O_2 stimulation in vitro reduced the level of SIRT1. SIRT1 is a NAD^+-dependent type III histone deacetylase, and it also deacetylates many other proteins. In response to stimulation, such as DNA damage or oxidative stress, proteins such as p53 and FOXO proteins are deacetylated, which impairs apoptosis (31). SIRT1 also plays a critical role in many pathological processes, including inflammation, stress resistance, and cellular senescence/aging (32, 33). Recently, emerging evidence has shown that SIRT1 levels are reduced in the lungs of patients and mice with COPD, which suggests the involvement of SIRT1 in the pathogenesis of COPD (20, 34, 35). Consistent with this, oxidative stress, such as that caused by H_2O_2, decreases the level of SIRT1 in vitro (34, 36). These findings suggest that FCHSD1 enhances alveolar inflammation and apoptosis by reducing SIRT1, which aggravates emphysema, although the possibility that decreased nuclear translocation of NRF2 by FCHSD1 may also directly contribute to the process cannot be excluded.

The regulatory role of SIRT1-NRF2 cross-talk in various processes has aroused researchers' interests. SIRT1 can regulate the level and activity of NRF2 (37), while NRF2 can regulate the level of SIRT1 (38, 39). Since our data indicate that FCHSD1 interacts with NRF2 but not with SIRT1, we conclude that NRF2 promotes SIRT1 levels and that FCHSD1 regulates this process. However, the underlying mechanism by which NRF2 regulates SIRT1 levels though FCHSD1–NRF2 interaction still needs further investigation.

Emerging evidence shows that activation of NRF2 is a promising therapeutic strategy. Indeed, bardoxolone methyl, the most potent known activator of the NRF2 pathway, reduces the serum creatinine concentration in patients with type 2 diabetes mellitus and chronic kidney disease (40). However, although it improves renal function, the phase 3 BEACON trial failed because bardoxolone methyl did not reduce the risk of end-stage renal disease, and many adverse events, including death from cardiovascular causes, were observed (41). SIRT1 is also considered a promising pharmaceutical target for the treatment of various diseases. For example, a potent SIRT1 activator, resveratrol, has been shown to extend the life span of various species (42) and to protect against metabolic disease (43). However, further studies are needed before it can be used clinically for certain diseases. The lung-specific expression and activity of FCHSD1 indicates that inhibition of FCHSD1 may contribute to a synergistic effect on NRF2- or SIRT1-targeted treatment, such as with bardoxolone methyl or resveratrol, and lower the risk of systemic adverse events.

In conclusion, our data provide insight into the role of FCHSD1 in stress-response sensing and as an integrator of oxidative stress. FCHSD1 reduced nuclear translocation of NRF2 and increased the reduction of SIRT1 levels, which are all ultimately involved in the pathogenesis of pulmonary emphysema. Our findings may also lead to a specific therapeutic strategy to ameliorate/halt the progression of emphysema via inhibition of FCHSD1.

Materials and Methods

Animal Husbandry and Ethics. Male mice (8- to 12-wk-old) were housed individually in ventilated cages in a temperature and light-regulated room in a specific pathogen-free facility and received food and water ad libitum. All studies received local ethics review board approval and were performed in accordance with the guidelines of the animal care and use committee of the Research Institute for Microbial Diseases at Osaka University.

Generation of *Fchsd1*$^{-/-}$ Mice. Oocytes and sperm were harvested from C57BL6/J mice and cultured together for 3 h in modified human tubal fluid medium. The fertilized eggs were washed using M2 medium and then 30 zygotes were collected and washed with Opti-MEM I three times to remove the serum in the medium. The zygotes were then electroporated using a CUY21EDIT II electroporator with a F501PT1-10 platinum plate electrode (length: 10 mm; width: 3 mm; height: 0.5 mm; gap: 1 mm) (BEX). The electrode was filled with 5 μL Opti-MEM I containing a mixture of Cas9 protein and single-guide RNA. After electroporation, the zygotes were immediately collected from the electrode chamber and washed with M2 medium four times. The eggs were then cultured in MWM medium at 37 °C in a 5% CO_2 incubator until the two-cell stage. These eggs were then transferred to the oviducts of pseudopregnant females on the day of the vaginal plug.

Experimental Emphysema. Groups of 8- to 12-wk-old male mice were anesthetized, and porcine pancreatic elastase (Fujifilm Wako Pure Chemical Corporation) at 4.2 U/kg body weight or saline alone were given intratracheally in a volume of 50 μL. Mice were killed at the indicated time points by terminal anesthesia for the collection of lungs and BAL fluid. Lungs samples were fixed for morphological evaluation.

Flow Cytometry and FACS. Cell suspensions were prepared by sieving and pipetting. Cells were washed in FACS buffer (0.5% bovine serum albumin [BSA] and 2 mM EDTA in PBS, pH 7.2), then incubated with antibodies for 20 min followed by washing twice with FACS buffer. Data were acquired on a flow cytometer (FACS CantoII, BD Bioscience) and analyzed using FlowJo (Tree Star) (44). Cells were sorted using a FACS Aria III (BD Bioscience). The following antibodies for flow cytometry and cell sorting were purchased from BioLegend: anti–Ly-6C (HK1.4), anti–Ly-6G (1A8), anti-Mac1 (M1/70), anti-CD45.2

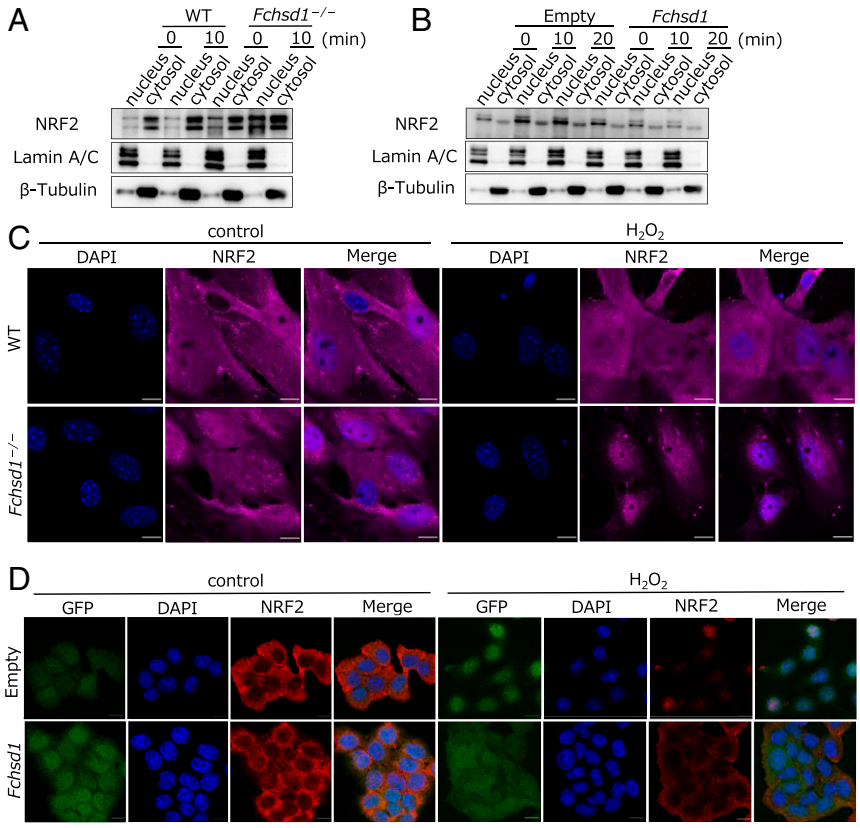

Fig. 5. FCHSD1 negatively regulates nuclear import of NRF2 in response to oxidative stress caused by H_2O_2. (*A*) Immunoblot analysis of nuclear and cytosol fractions of *Fchsd1*$^{-/-}$ and WT MLFs left untreated or treated with 275 μM H_2O_2 for 10 min. Data are representative of at least two independent experiments. (*B*) Immunoblot analysis of nuclear and cytosol fractions of MLE-12 cells transfected with retroviral *Fchsd1* or empty control vector left untreated or treated with 250 μM H_2O_2. Data are representative of at least two independent experiments. (*C*) Immunofluorescence detection of NRF2 (pink) in *Fchsd1*$^{-/-}$ and WT MLFs left untreated or treated with 275 μM H_2O_2 for 10 min. Original magnification, 62×. (Scale bars, 10 μm.) Data are representative of at least two independent experiments. (*D*) Immunofluorescence detection of NRF2 (red) and GFP (green) in MLE-12 cells transfected with retroviral *Fchsd1* or empty control vector left untreated or treated with 250 μM H_2O_2 for 10 min. Original magnification, 62×. (Scale bars, 10 μm.) Data are representative of at least two independent experiments.

(104), anti-CD11c (N418), anti-CD3e (145-2C11), anti-CD4 (GK1.5), anti-F4/80 (BM8), anti-SiglecF (S17007L), anti-CD8 (53-6.7), anti-CCR3 (J073E5), anti-B220 (RA3-6B2), anti-EpCAM (G8.8), anti-CD31 (MEC13.3), and anti-CD140a (APA5).

BAL and Analysis by Flow Cytometry and ELISA. Mice were analyzed at indicated time points. After making an incision in the trachea, a plastic cannula was inserted and airspaces were lavaged with 1 mL saline. This procedure was performed three times. After centrifugation, supernatant was used for cytokine measurement, and cells were used for cell determination. The cells were treated with red blood cell lysis buffer (Sigma-Aldrich) and washed with FACS buffer. Cell determination data of Mac1$^+$ Ly6c$^+$ Ly6g$^+$ neutrophils were acquired using a FACS Canto II flow cytometer and analyzed by FlowJo software as described above. Commercial ELISA kits (R&D Biosystems) were used to measure total TNF-α and IL-6 in the indicated samples, in accordance with the manufacturer's instructions.

LPS-Induced Lung Inflammation and Injury Model. Male mice (8 to 12 wk of age) were intratracheally instilled with LPS from *Salmonella minnesota* R595 (10 mg/kg body weight; Invivogen). After 24 h, BAL fluid was collected for cell counts and analysis of cytokines. For mortality studies, mice were monitored every day for up to 15 d.

Cell Isolation and Culture. Primary lung fibroblasts (MLFs) were isolated from WT and *Fchsd1*$^{-/-}$ mice using trypsin digestion, and the cells were grown in DMEM supplemented with 10% fetal calf serum (no. 10270-106; Gibco), 100 U/mL penicillin G, 100 μg/mL streptomycin (both from Nacalai Tesque), and 2-mercaptoethanol (no. 21417-52; Nacalai Tesque) in a 5% CO_2, 95% O_2 atmosphere at 37 °C. Mouse type II alveolar epithelial cells (MLE-12) were cultured in DMEM Ham's F-12 medium (no. 08460-95; Nacalai Tesque) supplemented with 2% fetal calf serum (no. 10270-106; Gibco), 100 U/mL penicillin G, 100 μg/mL streptomycin (both from Nacalai Tesque), 0.005 mg/mL insulin (no. 2585; Gibco), 0.01 mg/mL transferrin (no. T5391; Sigma Aldrich), 30 nM sodium selenite (no. S9133; Sigma Aldrich), 10 nM hydrocortisone (no. H0135; Sigma Aldrich), 10 nM β-estradiol (no. E2257; Sigma Aldrich), 10 mM Hepes (no. H0887; Sigma Aldrich), and 2 mM L-glutamine (no. 250030; Gibco). Alveolar macrophages represented >95% of cells in the BAL of unchallenged C57BL/6 mice and were recovered as described above. MLFs were used up to passage 3, while MLE-12 cells were used up to passage 10. The treatments used were: H_2O_2 50 to 275 μM (no. 7722-84-1; Santoku Chemical Industries), LPS 1 μg/mL (no. tlrl-smlps; Invivogen), and Pam3CSK4 1 μg/mL (no. tlrl-pms; Invivogen). Primary lung cells were prepared as described previously (45). Briefly, lungs were excised from mice and cut into small pieces, then cells were dissociated from lung tissues with collagenase I (1 mg/mL; Sigma). The single-cell suspensions were stained with antibodies as described above, and then epithelial cells (defined as lung CD45$^-$ CD31$^-$ EpCAM1$^+$ cells), fibroblasts (defined as lung CD45$^-$ CD31$^-$ EpCAM1$^-$ CD140a$^+$ cells), endothelial cells (defined as lung CD45$^-$ CD31$^+$ EpCAM1$^-$ CD140a$^-$ cells), and macrophages (defined as lung CD45$^+$ CD11c$^+$ Mac1$^+$ cells) were sorted using a FACS Aria III.

Construction of Expression Plasmids. *Fchsd1*, *Nrf2*, and *Snx9* cDNAs were obtained by PCR from a mouse cDNA library. *Fchsd1* cDNAs were cloned into pLZR-ires-GFP for retrovirus production. Flag-tagged *Fchsd1*, Flag-tagged *Nrf2*, HA-tagged *Nrf2*, Flag-tagged *Snx9*, and Myc-tagged *Snx9* were cloned into pcDNA3.1(+) for immunoprecipitation.

Retroviral Transduction. MLE-12 cells were transduced with retroviral supernatant. Virus was produced using PlatE packaging cells transfected with pLZR-ires-GFP containing a full-length *Fchsd1* cDNA or empty vector. After transduction, GFP$^+$ cells were sorted using a FACS Aria III (44).

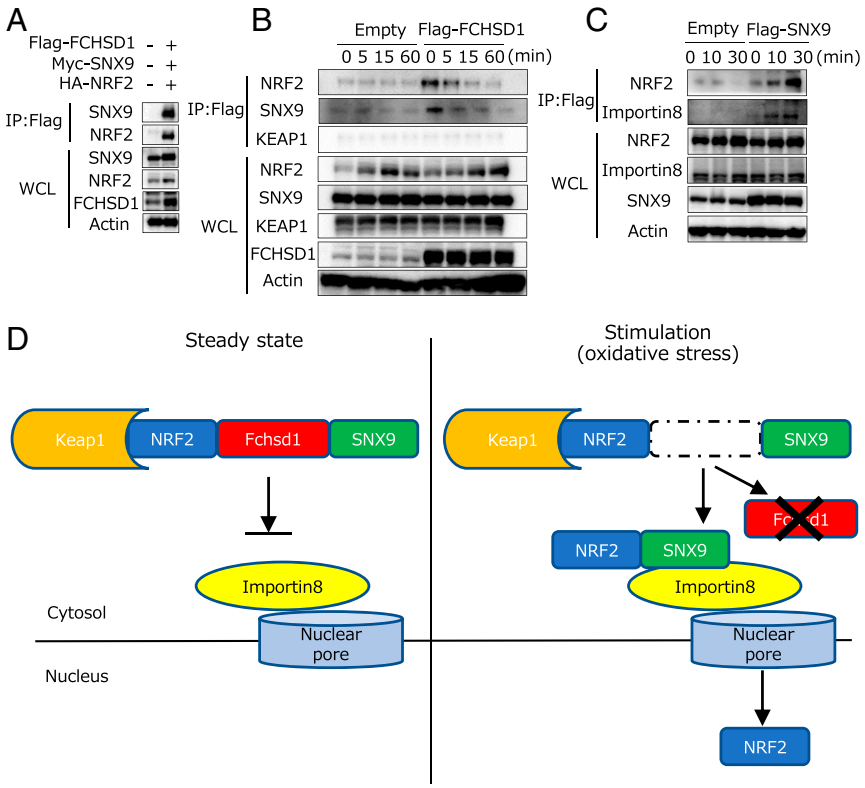

Fig. 6. FCHSD1 interacts with NRF2 and SNX9, but not with Importin 8, while SNX9 interacts with NRF2 and Importin 8. (*A*) MLE12 cells were transfected with Flag-tagged FCHSD1, Myc-tagged SNX9, and HA-tagged NRF2, or empty vector and immunoprecipitated (IP) with anti-Flag resin before western analysis for bound NRF2 or SNX9. In the bottom, whole-cell lysate (WCL) was immunoblotted for the indicated targets. Data are representative of at least two independent experiments. (*B*) Immunoblot analysis of MLE-12 cells expressing Flag-tagged FCHSD1 or empty vector and immunoprecipitation with anti-Flag resin in response to oxidative stress caused by 250 μM H_2O_2 treatment for the indicated times. Data are representative of at least two independent experiments. (*C*) Immunoblot analysis of MLE-12 cells expressing Flag-tagged SNX9, or empty vector and immunoprecipitation with anti-Flag resin in response to oxidative stress caused by 250 μM H_2O_2 treatment for the indicated times. Data are representative of at least two independent experiments. (*D*) In the nonstimulated state, FCHSD1 forms complexes with NRF2 and SNX9 in the cytosol and prevents NRF2 from translocating to the nucleus. NRF2 is also bound to KEAP1, its endogenous inhibitor, and is targeted for proteasomal degradation. In response to oxidative stress, KEAP1 is modified and stabilizes NRF2. Then, FCHSD1 dissociates from the complex and SNX9 bound to nuclear membrane-associated Importin 8 targets NRF2 to the nuclear pore.

Quantitative Reverse-Transcription PCR. Total RNA was isolated using an RNA purification kit (no. 1828665; Roche) or TRIzol (no. 15596018; Thermo Fisher Scientific) and reverse transcription was performed with ReverTraAce (Toyobo) according to the manufacturer's instructions. Quantitative reverse-transcription PCR (RT-qPCR) was performed using real-time PCR Master mix (Toyobo), and fluorescence from the TaqMan probe for each gene was detected with a 7500 real-time PCR system (Applied Biosystems). To determine the relative induction of mRNA, the mRNA level of each gene was calculated using the standard curve method normalized to 18S. Commercially available gene-specific primers and probe sets were obtained from Integrated DNA Technologies (Coralville). The primers and probes used in the study were: *Il6* (Mm.PT.58.10005566), *Tnfa* (Mm.PT.58.12575861), and *Nrf2* (Mm.PT.58.29108649).

Western Blotting. Cultured cells and primary cells were lysed with lysis buffer (20 mM Tris·HCl [pH 7.5], 150 mM NaCl, 1 mM EDTA and 1% [vol/vol] Nonidet P-40) containing cOmplete Mini Protease Inhibitor Mixture (Roche), and tissue samples were homogenized in RIPA buffer (no. 08714; Nacalai Tesque) at 1:10 (wt/vol) then centrifuged to pellet cell/tissue debris. The lysates were separated by standard SDS/PAGE and analyzed by immunoblotting. Antibodies to the following proteins were used: SIRT1 (no. 9475; Cell Signaling Technology), FCHSD1 (no. 23362-1-AP; Proteintech), PPARγ (no. 2443; Cell Signaling Technology), NRF2 (no. 12721; Cell Signaling Technology), Lamin A/C (no. 2032; Cell Signaling Technology), β-tubulin (no. 2128; Cell Signaling Technology), WRP (no. E-AB-11600; Elabscience), TOCA-1 (no. E-AB-19876; Elabscience), FER (no. E-AB-19864; Elabscience), CIP4 (no. E-AB-61483; Elabscience), FCHSD2 (no. orb183665; biorbyt), Importin 8 (no. ab208162; Abcam), Importin α5 (no. 18137-1-AP; Proteintech), SNX9 (no. 15721-1-AP; Proteintech), Importin β1 (no. 51186; Cell Signaling Technology), KPNA2 (no. 14372; Cell Signaling Technology), β-actin (no. sc-47778; Santa Cruz Biotechnology), cleaved caspase-3 (no. 9664; Cell Signaling Technology), caspase-3 (no. 9662; Cell Signaling Technology), and Acetyl-p53 (no. 2570; Cell Signaling Technology).

Histological Analysis. Each organ was rapidly excised, fixed with 4% paraformaldehyde for 24 h, and embedded in paraffin. Tissue sections (5-μm thick) were prepared using a paraffin microtome, deparaffinized with xylene, dehydrated through a graded ethanol series, and processed for hematoxylin and eosin (H&E) staining. The slides stained with H&E were used to evaluate pulmonary emphysema. Percentages of lung tissue affected by emphysema in whole lung were measured using a BZ-X710 fluorescence microscope (Keyence Corp.) and the images were processed and reconstructed using BZ-X Analyzer software in accordance with the manufacturer's instructions. All quantitative measurements were performed in comparable areas under the same optical and light conditions. For the evaluation of pulmonary emphysema, the MLI was measured after H&E staining using ImageJ software.

Immunocytochemistry. Cells were cultured on coverslips, fixed with 4% PFA, permeabilized with 0.2% Triton X-100 in PBS and blocked with 1% BSA in PBS containing 0.1% Tween20. Cells were then incubated with primary and secondary antibodies and imaged with a confocal microscope (LSM 880, Zeiss) (45). Antibodies to the following proteins were used: NRF2 (no. 16396-1-AP; Proteintech) and Alexa Fluor 647–conjugated goat anti-rabbit IgG (no. A21245; Invitrogen), as well as Hoechst33342 (no. H342; Dojindo).

Transfection and Immunoprecipitation. MLE-12 cells were transfected with pcDNA3.1 (+) encoding Flag-tagged *Fchsd1*, Flag-tagged *Nrf2*, HA-tagged *Nrf2*, Flag-tagged *Snx9*, and Myc-tagged *Snx9* or empty vector using Lipofectamine 2000 (no. 11668027; Thermo Fisher Scientific). Twenty-four hours

after transfection, cell lysates were collected. For immunoprecipitation with an anti-Flag antibody, cells were lysed in lysis buffer (20 mM Tris·HCl [pH 7.5], 150 mM NaCl, and 1% [vol/vol] Nonidet P-40) containing cOmplete Mini Protease Inhibitor Mixture (Roche). Cell lysates were incubated for 2 h with anti-Flag M2 affinity gel (no. A2220; Sigma Aldrich), and washed in wash buffer (20 mM Tris·HCl [pH 7.5] and 150 mM NaCl). Proteins were separated by standard SDS/PAGE and analyzed by immunoblotting.

Magnetic Resonance Imaging. An AvanceIII BioSpec 117/11 system (Bruker) equipped with a 1H QD coil was used for MRI imaging (46). Mice were anesthetized with sevoflurane during image acquisition and the mouse body temperature was maintained with a warm water circulating tube. An ultrashort echo time imaging method was used for lung imaging with the following parameters: TR/TE = 5/0.1 ms, field of view 3 cm, and slice thickness 0.15 mm. Image matrix was set to 200 × 200 × 200.

Subcellular Fractionation. For subcellular fractionation, MLFs or MLE-12 cells were plated at 1.2×10^6 cells per dish. Cells were stimulated with 275 μM H_2O_2 (for MLFs) or 250 μM H_2O_2 (for MLE12 cells) for the indicated times. After stimulation, cell extracts were prepared using a Nuclear extract kit (no. 40010; Active Motif), in accordance with the manufacturer's instructions.

Statistical Analysis. Data from two independent groups were analyzed by Student's *t* test. Survival data were analyzed by the log-rank test. For all tests, a *P* value of less than 0.05 was considered statistically significant.

Data Availability. All study data are included in the article and *SI Appendix*.

ACKNOWLEDGMENTS. We thank N. Miyamoto, R. Takenaka, T. Hongo, and K. Yamada for assistance with the experiments; E. Kamada for secretarial assistance; C. Funamoto, K. Yokoyama, and R. Kawaguchi for technical assistance; and Jeremy Allen, from the Edanz Group (https://www.edanz.com/ac) for editing a draft of this manuscript. This work was supported by the Japan Science and Technology Agency (JST) through funding for Specially Promoted Research (15H05704), a Grant-in-Aid for Young Scientists (A) (16H06234), a Grant-in-Aid for Challenging Exploratory Research (T17K195570), and a Grant-in-Aid for Scientific Research on Innovative Areas (18H05032). This work was also supported by the Visionary Research Fund from Takeda Science Foundation and the Joint research chair of innate immunity supported by Otsuka Pharmaceutical Co., Ltd. This work was also supported by PRIME (17gm6110002h0001), ACT-M (17im0210108h0001), and the Research Program on Hepatitis (18fk0310106h0002 and 18fk0210041h0001) from the Japan Agency for Medical Research and Development, AMED.

1. P. J. Barnes *et al*., Chronic obstructive pulmonary disease. *Nat. Rev. Dis. Primers* **1**, 15076 (2015).
2. R. M. Tuder, T. Yoshida, W. Arap, R. Pasqualini, I. Petrache, State of the art. Cellular and molecular mechanisms of alveolar destruction in emphysema: An evolutionary perspective. *Proc. Am. Thorac. Soc.* **3**, 503–510 (2006).
3. R. M. Tuder *et al*., Oxidative stress and apoptosis interact and cause emphysema due to vascular endothelial growth factor receptor blockade. *Am. J. Respir. Cell Mol. Biol.* **29**, 88–97 (2003).
4. R. F. Foronjy *et al*., Superoxide dismutase expression attenuates cigarette smoke- or elastase-generated emphysema in mice. *Am. J. Respir. Crit. Care Med.* **173**, 623–631 (2006).
5. T. Kinoshita *et al*., Thioredoxin prevents the development and progression of elastase-induced emphysema. *Biochem. Biophys. Res. Commun.* **354**, 712–719 (2007).
6. A. Csordas *et al*., Cigarette smoke extract induces prolonged endoplasmic reticulum stress and autophagic cell death in human umbilical vein endothelial cells. *Cardiovasc. Res.* **92**, 141–148 (2011).
7. M. M. Monick *et al*., Identification of an autophagy defect in smokers' alveolar macrophages. *J. Immunol.* **185**, 5425–5435 (2010).
8. R. M. Tuder, I. Petrache, Pathogenesis of chronic obstructive pulmonary disease. *J. Clin. Invest.* **122**, 2749–2755 (2012).
9. N. Mercado, K. Ito, P. J. Barnes, Accelerated ageing of the lung in COPD: New concepts. *Thorax* **70**, 482–489 (2015).
10. D. Singh *et al*., Global strategy for the diagnosis, management, and prevention of chronic obstructive lung disease: The GOLD science committee report 2019. *Eur. Respir. J.* **53**, 1900164 (2019).
11. M. N. Teruel, T. Meyer, Translocation and reversible localization of signaling proteins: A dynamic future for signal transduction. *Cell* **103**, 181–184 (2000).
12. T. Itoh *et al*., Dynamin and the actin cytoskeleton cooperatively regulate plasma membrane invagination by BAR and F-BAR proteins. *Dev. Cell* **9**, 791–804 (2005).
13. N. Kogata *et al*., Identification of Fer tyrosine kinase localized on microtubules as a platelet endothelial cell adhesion molecule-1 phosphorylating kinase in vascular endothelial cells. *Mol. Biol. Cell* **14**, 3553–3564 (2003).
14. K. Takano, K. Toyooka, S. Suetsugu, EFC/F-BAR proteins and the N-WASP-WIP complex induce membrane curvature-dependent actin polymerization. *EMBO J.* **27**, 2817–2828 (2008). Corrected in: *EMBO J.* **27**, 3332 (2008).
15. B. R. Carlson *et al*., WRP/srGAP3 facilitates the initiation of spine development by an inverse F-BAR domain, and its loss impairs long-term memory. *J. Neurosci.* **31**, 2447–2460 (2011).
16. G. Y. Xiao, A. Mohanakrishnan, S. L. Schmid, Role for ERK1/2-dependent activation of FCHSD2 in cancer cell-selective regulation of clathrin-mediated endocytosis. *Proc. Natl. Acad. Sci. U.S.A.* **115**, E9570–E9579 (2018).
17. M. Katoh, M. Katoh, Identification and characterization of human FCHSD1 and FCHSD2 genes in silico. *Int. J. Mol. Med.* **13**, 749–754 (2004).
18. K. M. O'Connor-Giles, L. L. Ho, B. Ganetzky, Nervous wreck interacts with thick veins and the endocytic machinery to attenuate retrograde BMP signaling during synaptic growth. *Neuron* **58**, 507–518 (2008).
19. X. Sun *et al*., Transcription factor Sp4 regulates expression of nervous wreck 2 to control NMDAR1 levels and dendrite patterning. *Dev. Neurobiol.* **75**, 93–108 (2015).
20. H. Yao *et al*., SIRT1 protects against emphysema via FOXO3-mediated reduction of premature senescence in mice. *J. Clin. Invest.* **122**, 2032–2045 (2012).
21. H. Cao *et al*., FCHSD1 and FCHSD2 are expressed in hair cell stereocilia and cuticular plate and regulate actin polymerization in vitro. *PLoS One* **8**, e56516 (2013).
22. T. Li *et al*., Resveratrol reduces acute lung injury in a LPS-induced sepsis mouse model via activation of Sirt1. *Mol. Med. Rep.* **7**, 1889–1895 (2013).
23. C. Y. Sun *et al*., Protective effects of pogostone against LPS-induced acute lung injury in mice via regulation of Keap1-Nrf2/NF-κB signaling pathways. *Int. Immunopharmacol.* **32**, 55–61 (2016).
24. R. K. Thimmulappa *et al*., Nrf2-dependent protection from LPS induced inflammatory response and mortality by CDDO-Imidazolide. *Biochem. Biophys. Res. Commun.* **351**, 883–889 (2006).
25. M. Yamamoto, T. W. Kensler, H. Motohashi, The KEAP1-NRF2 system: A thiol-based sensor-effector apparatus for maintaining redox homeostasis. *Physiol. Rev.* **98**, 1169–1203 (2018).
26. Y. Ishii *et al*., Transcription factor Nrf2 plays a pivotal role in protection against elastase-induced pulmonary inflammation and emphysema. *J. Immunol.* **175**, 6968–6975 (2005).
27. T. Rangasamy *et al*., Genetic ablation of Nrf2 enhances susceptibility to cigarette smoke-induced emphysema in mice. *J. Clin. Invest.* **114**, 1248–1259 (2004).
28. M. Theodore *et al*., Multiple nuclear localization signals function in the nuclear import of the transcription factor Nrf2. *J. Biol. Chem.* **283**, 8984–8994 (2008).
29. N. S. Rajasekaran *et al*., Sustained activation of nuclear erythroid 2-related factor 2/antioxidant response element signaling promotes reductive stress in the human mutant protein aggregation cardiomyopathy in mice. *Antioxid. Redox Signal.* **14**, 957–971 (2011).
30. K. Taguchi *et al*., Keap1 degradation by autophagy for the maintenance of redox homeostasis. *Proc. Natl. Acad. Sci. U.S.A.* **109**, 13561–13566 (2012).
31. R. H. Houtkooper, E. Pirinen, J. Auwerx, Sirtuins as regulators of metabolism and healthspan. *Nat. Rev. Mol. Cell Biol.* **13**, 225–238 (2012).
32. J. W. Hwang, H. Yao, S. Caito, I. K. Sundar, I. Rahman, Redox regulation of SIRT1 in inflammation and cellular senescence. *Free Radic. Biol. Med.* **61**, 95–110 (2013).
33. I. B. Leibiger, P. O. Berggren, Sirt1: A metabolic master switch that modulates lifespan. *Nat. Med.* **12**, 34–36, discussion 36 (2006).
34. Y. Nakamaru *et al*., A protein deacetylase SIRT1 is a negative regulator of metalloproteinase-9. *FASEB J.* **23**, 2810–2819 (2009).
35. S. Rajendrasozhan, S. R. Yang, V. L. Kinnula, I. Rahman, SIRT1, an antiinflammatory and antiaging protein, is decreased in lungs of patients with chronic obstructive pulmonary disease. *Am. J. Respir. Crit. Care Med.* **177**, 861–870 (2008).
36. S. Caito *et al*., SIRT1 is a redox-sensitive deacetylase that is post-translationally modified by oxidants and carbonyl stress. *FASEB J.* **24**, 3145–3159 (2010).
37. S. R. Kulkarni *et al*., Fasting induces nuclear factor E2-related factor 2 and ATP-binding Cassette transporters via protein kinase A and Sirtuin-1 in mouse and human. *Antioxid. Redox Signal.* **20**, 15–30 (2014).
38. K. Huang, X. Gao, W. Wei, The crosstalk between Sirt1 and Keap1/Nrf2/ARE anti-oxidative pathway forms a positive feedback loop to inhibit FN and TGF-β1 expressions in rat glomerular mesangial cells. *Exp. Cell Res.* **361**, 63–72 (2017).
39. D. S. Yoon, Y. Choi, J. W. Lee, Cellular localization of NRF2 determines the self-renewal and osteogenic differentiation potential of human MSCs via the P53-SIRT1 axis. *Cell Death Dis.* **7**, e2093 (2016).
40. P. E. Pergola *et al*.; BEAM Study Investigators, Bardoxolone methyl and kidney function in CKD with type 2 diabetes. *N. Engl. J. Med.* **365**, 327–336 (2011).
41. D. de Zeeuw *et al*.; BEACON Trial Investigators, Bardoxolone methyl in type 2 diabetes and stage 4 chronic kidney disease. *N. Engl. J. Med.* **369**, 2492–2503 (2013).
42. B. Rogina, S. L. Helfand, Sir2 mediates longevity in the fly through a pathway related to calorie restriction. *Proc. Natl. Acad. Sci. U.S.A.* **101**, 15998–16003 (2004).
43. M. Lagouge *et al*., Resveratrol improves mitochondrial function and protects against metabolic disease by activating SIRT1 and PGC-1alpha. *Cell* **127**, 1109–1122 (2006).
44. T. Satoh *et al*., Critical role of Trib1 in differentiation of tissue-resident M2-like macrophages. *Nature* **495**, 524–528 (2013).
45. K. Fukushima *et al*., Dysregulated expression of the nuclear exosome targeting complex component Rbm7 in nonhematopoietic cells licenses the development of fibrosis. *Immunity* **52**, 542–556.e13 (2020).
46. T. Satoh *et al*., Identification of an atypical monocyte and committed progenitor involved in fibrosis. *Nature* **541**, 96–101 (2017).